land

MDPI

Article

Increased Sensitivity of Alpine Grasslands to Climate Change on the Tibetan Plateau

Zhuanjia Xu [1], Lanhui Li [1,2,*], Binghua Zhang [2], Shuimei Fu [1], Wei Liu [1], Yanran Luo [1], Hui Li [1], Xiaoling Zhu [1] and Fuliang Deng [1]

[1] School of Computer and Information Engineering, Xiamen University of Technology, Xiamen 361024, China; 2322071043@stu.xmut.edu.cn (Z.X.); 2422071011@stu.xmut.edu.cn (S.F.); devilweil@xmut.edu.cn (W.L.); 2110903136@stu.xmut.edu.cn (Y.L.); lih666@xmut.edu.cn (H.L.); zhuxl@xmut.edu.cn (X.Z.); fldeng8266@xmut.edu.cn (F.D.)

[2] Key Laboratory of Land Surface Pattern and Simulation, Institute of Geographic Sciences and Natural Resources Research, CAS, Beijing 100101, China; zhangbh.17b@igsnrr.ac.cn

* Correspondence: lilh.15b@igsnrr.ac.cn

Abstract

Accurately quantifying the sensitivity of alpine vegetation to climate change is a key prerequisite for formulating regional climate change adaptation policies. The sensitivity of the fragile alpine grasslands on the Tibetan Plateau to climate change has received widespread attention. However, the spatiotemporal dynamics and driving mechanisms of this sensitivity are still unclear under continuous warming and wetting. This study, based on MODIS_NDVI and meteorological data from 2000 to 2023, constructed a dynamic Vegetation Sensitivity Index (VSI) framework and integrated Random Forest (RF) and eXtreme Gradient Boosting (XGBoost) models with Shapley Additive exPlanations (SHAP) attribution analysis to reveal the spatiotemporal evolution characteristics and driving mechanisms of vegetation sensitivity on the Tibetan Plateau. The results show that (1) the VSI of alpine grasslands exhibited a spatial pattern of higher values in the southwest and lower values in the northeast, with an overall upward trend. Specifically, 56.31% of the region showed an increase in the VSI, with the upward trend being more pronounced in the northern plateau. (2) The dominant role of different climate factors varied regionally; vegetation sensitivity to precipitation increased in the northern plateau, and temperature sensitivity decreased in the central plateau, while sensitivity to solar radiation significantly increased in the central plateau. (3) SHAP attribution analysis indicated that elevation was the core factor driving VSI differentiation, showing a higher sensitivity at higher elevations, with lower growth rates. These findings reveal the dynamic evolution of vegetation sensitivity under the warming and wetting climate trend and its elevation-regulated mechanism, providing important scientific insights for regional ecological adaptation management.

Keywords: Tibetan Plateau; Vegetation Sensitivity Index; elevation gradient; climate change; machine learning

Check for updates

Academic Editor: Yongheng Gao

Received: 28 December 2025
Revised: 20 January 2026
Accepted: 22 January 2026
Published: 26 January 2026

Copyright: © 2026 by the authors. Licensee MDPI, Basel, Switzerland. This article is an open access article distributed under the terms and conditions of the Creative Commons Attribution (CC BY) license.

1. Introduction

The Tibetan Plateau, known as the "Roof of the World", hosts a unique high-elevation ecosystem and plays a crucial role in regulating regional and even global climate and hydrological cycles [1–3]. The plateau is experiencing intense warming, significantly exceeding the global average, posing a threat to the stability of alpine ecosystems [4,5]. Vegetation dynamics are a key indicator of ecosystem responses to climate change [6], and climate

change is a primary driver of vegetation shifts on the plateau [7,8]. Therefore, accurately quantifying the sensitivity of vegetation to climate change and understanding its spatiotemporal evolution is critical for predicting ecosystem changes under future climate scenarios and for formulating scientifically sound and effective adaptation management strategies.

The sensitivity of ecosystems to climate change has received widespread attention, and many quantitative methods have been proposed. For example, Piao et al. [9] calculated the interannual variation trend and correlation coefficient of NDVI with factors such as precipitation and temperature, and preliminarily revealed the response intensity of temperate grasslands in China to climate change. Chen et al. [10] used a long short-term memory network deep learning model to quantify the sensitivity of global vegetation to climate factors by simulating the nonlinear response of global vegetation to climate factors. However, while these methods reveal general patterns or non-linear relationships, they often overlook ecosystem stability. Unlike simple trend analyses that mask volatility and potential vulnerability [11], or categorical methods that simplify dynamic processes, a continuous sensitivity index is superior in quantifying the non-stationary nature of vegetation–climate coupling [12]. In this context, Seddon et al. [6] combined Principal Component Regression (PCR) with an autoregressive model to quantify and integrate the sensitivity of vegetation variability to climate variability and the relative contribution weights of various climate factors. Using monthly scale satellite remote sensing vegetation index data and multiple climate factor datasets, they constructed a spatially comparable Vegetation Sensitivity Index (VSI). Li et al. [13] improved the method and studied the vegetation sensitivity of the Tibetan Plateau and pointed out that the southern plateau is generally more sensitive to climate variability in terms of spatial pattern, and the sensitivity increases with the elevation gradient. However, this study only focused on 2000–2015; it remains unclear whether this spatial pattern persists to the present day and whether the sensitivity differences in the region are still influenced by elevation.

As global climate change intensifies [14–17], the sensitivity of alpine grasslands ecosystems to climate exhibits dynamic evolutionary characteristics [18,19]. In arid regions worldwide, vegetation sensitivity to climate variability, particularly precipitation, shows a significant upward trend, while in humid regions, it has decreased [20,21]. In China, over the past three decades, more than 23% of vegetation areas have experienced significant interannual variability in sensitivity, with solar radiation, temperature, and precipitation having different driving effects across various climate zones [22]. Notably, in the arid and semi-arid regions of Northern China, ecosystem vulnerability responds strongly to trends in desertification. Under dry conditions, ecosystem resilience significantly decreases compared to wet conditions, leading to increased sensitivity [23]. Under the accelerated warming and wetting climate trend [24], how does the sensitivity of alpine vegetation on the Tibetan Plateau evolve? Is this trend more pronounced at higher elevation? These questions require further validation.

This study aimed to explore the changing characteristics of alpine vegetation sensitivity to climate change on the Tibetan Plateau. Specifically, we proposed the following hypotheses: (1) vegetation sensitivity to climate shows significant increased trends under prolonged warming and wetting; and (2) elevation gradients nonlinearly modulate the vegetation–climate relationship, with threshold effects or transitional zones at certain altitudes. To test these hypotheses, this study (1) employed a multi-time-window sliding analysis technique to track the spatiotemporal evolution trajectory and robustness characteristics of vegetation sensitivity on the Tibetan Plateau from 2000 to 2023 and (2) investigated the nonlinear regulatory mechanism of elevation gradients on the relationship of vegetation–climate sensitivity. The results will help clarify the dynamic response of plateau ecosystems to climate change in the context of warming and wetting, providing a

solid scientific foundation for the adaptive management of regional ecological barriers and adjustments to ecological red lines.

2. Materials and Methods

2.1. Study Area

The Tibetan Plateau, located between 73°19′ to 104°47′ E and 26°00′ to 39°47′ N (Figure 1), is the largest and highest plateau on Earth, covering an area of approximately 257×10^4 km^2 [25]. It is known as the "Third Pole" and the "Water Tower of Asia" [26,27]. With an average elevation exceeding 4000 m, its huge elevation and vast area have an extremely important driving and amplifying effect on regional and even global atmospheric circulation and climate systems [28]. The plateau exhibits typical alpine climate characteristics, with significant spatial variation. Both average temperature and precipitation decrease from the southeast to the northwest. Most areas have an annual average temperature below 0 °C [29], and annual precipitation ranges from 50 to 1000 mm [30]. The ecological environment is unique and fragile, with a complex climate influenced significantly by elevation and topography. The plateau supports diverse ecosystems, including subtropical forests, broadleaf and coniferous forests, agricultural lands, and grassland vegetation, with grasslands dominating the region. Grasslands cover 60% of the vegetation in the area [31].

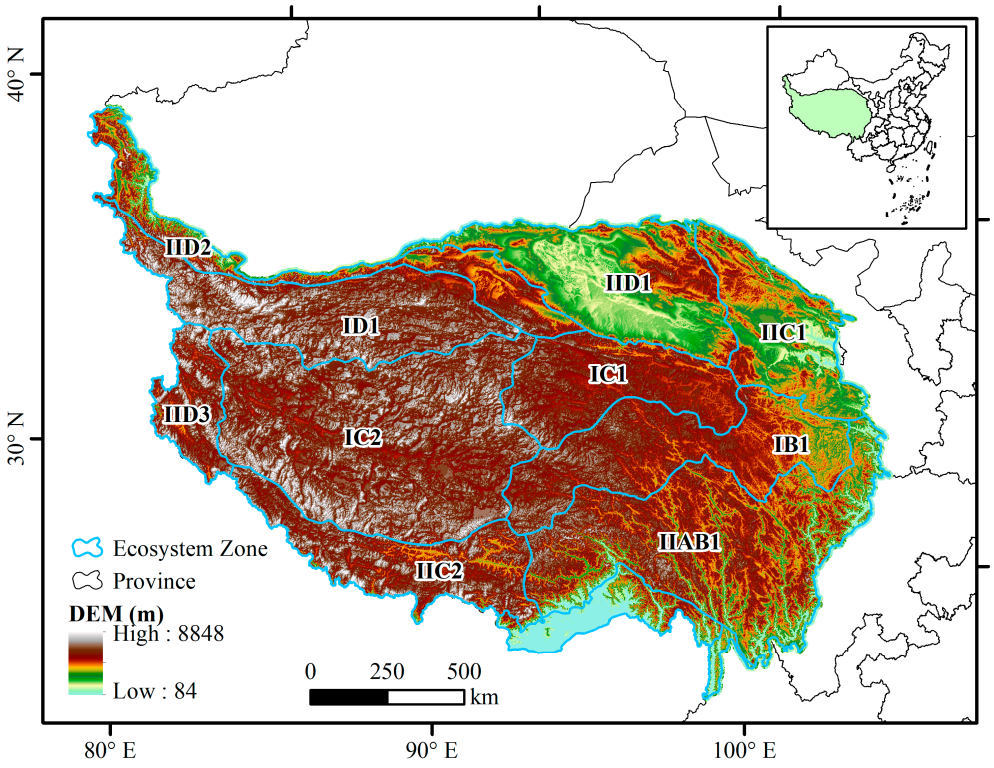


Figure 1. The ecosystem zonation of the Tibetan Plateau, which includes the following regions: the temperate humid/sub-humid western Sichuan–eastern Tibet montane coniferous forest zone (IIAB1), sub-cold sub-humid Guoluo–Naqu mountain alpine shrub-meadow zone (IB1), temperate semi-arid eastern Qinghai–Qilian montane steppe zone (IIC2), sub-cold semi-arid southern Qinghai alpine meadow-steppe (IC1), Qiangtang alpine steppe zones (IC2), temperate semi-arid southern Tibet montane shrub-steppe zone (IIC1), temperate arid Qaidam Basin desert region (IID2), temperate arid north Kunlun desert zone (IID3), sub-cold arid Kunlun mountain and plateau alpine steppe zone (ID1), and temperate arid Ngali montane desert zone (IID1).

2.2. Data Sources and Preprocessing

2.2.1. NDVI Data

This study uses the sixth edition of the MODIS_NDVI product, covering the period from 2000 to 2023 (Table 1), as the data source and explores the variation characteristics of vegetation greenness in the alpine region of the Tibetan Plateau by characterizing vegetation greenness using the NDVI index. To improve data quality, the Savitzky–Golay filtering algorithm of the TIMESAT software package (version 3.3) in the MATLAB environment was used for noise reduction to address the noise problem caused by cloud, snow, and ice cover. During the noise reduction process, the quality factor of the MODIS VI dataset was incorporated as a harmonic coefficient into the processing flow, thereby enhancing the reliability and stability of NDVI data reconstruction.

Table 1. Datasets used in this study and their characteristics.

Data Type	Variable	Dataset Name	Resolution	Data Source
Vegetation Data	NDVI	MODIS_ NDVI	1 km	https://www.earthdata.nasa.gov/data/catalog/lpcloud-mod13a2-061 (accessed on 27 December 2025)
Meteorological Data	Temperature Cumulative Precipitation Solar Radiation	A high-resolution near-surface meteorological forcing dataset for the Third Pole region	1/30°	https://data.tpdc.ac.cn/en/data/44a449ce-e660-44c3-bbf2-31ef7d716ec7 (accessed on 27 December 2025)
	Vapor Pressure Deficit	TerraClimate	1/24°	https://climatedataguide.ucar.edu/climate-data/terraclimate-global-high-resolution-gridded-temperature-precipitation-and-other-water (accessed on 27 December 2025)
Auxiliary Data	Aridity Index	1 km annual arid index dataset for China	1/24°	https://doi.org/10.11888/Atmos.tpdc.300560 (accessed on 27 December 2025)
	Carbon Dioxide	Global 1 km resolution atmospheric carbon dioxide concentration dataset	1 km	https://data.tpdc.ac.cn/en/data/9dddf566-72ce-4a1e-9b2b-5998e38df3a5 (accessed on 27 December 2025)
	Soil Organic Carbon	Basic soil property dataset of high-resolution China Soil Information Grids	1 km	http://doi.org/10.11666/00073.ver1.db (accessed on 27 December 2025)
	Elevation	Shuttle Radar Topography Mission	300 m	https://www.resdc.cn/data.aspx?DATAID=217 (accessed on 27 December 2025)

2.2.2. Meteorological and Environmental Driving Data

The meteorological grid data used in this study are sourced from the high-resolution near-surface meteorological forcing dataset for the Third Pole region, which includes daily, monthly, and annual mean temperature, precipitation, solar radiation, and other meteorological elements from 1979 to the present (Table 1). This dataset was obtained by downscaling ERA5 data using high-resolution Random Forest (RF) simulations and machine learning algorithms, then integrating high-density ground station data. The downward shortwave radiation data were generated by applying quality homogenization processing to satellite-derived shortwave radiation using ERA5 data. The spatial resolution of this dataset is 1/30°, and it has been used for climate analysis in the Third Pole region as well as for inputs to land, hydrological, and ecological models [32,33]. To construct a spatially consistent dataset for pixel-level analysis, we standardized all meteorological data to match the 1 km spatial resolution of the MODIS NDVI dataset. Specifically, for continuous meteorological and environmental variables, we employed bilinear interpolation for resampling. This method was selected to ensure smooth spatial transitions while preserving the detailed topographic climate patterns already embedded in the high-resolution source datasets [34]. Similar resampling methods were applied to auxiliary data. In addition, to comprehensively assess the impact of moisture stress and soil environment on vegetation, this study incorporated the following environmental variables: (1) Vapor Pressure Deficit data, sourced from the TerraClimate dataset [35]; (2) Aridity Index and Carbon Dioxide, obtained from the National Tibetan Plateau Scientific Data Center [36]; (3) Soil Organic

Carbon content data, sourced from the National Earth System Science Data Center [37]; (4) elevation data, obtained from the Chinese Academy of Sciences Resource and Environmental Science Data Platform; and (5) Human Activity Index data, calculated in this study by integrating stressors like grazing and roads [38].

2.3. Research Methods

To quantitatively characterize the sensitivity of the Tibetan Plateau ecosystems to climate change, this study adapts the ecosystem climate sensitivity analysis framework proposed by Seddon et al. [6], incorporating modifications to account for regional characteristics such as high elevation, short growing seasons, and poor water–energy matching (Figure 2). Specifically, we focus on data analysis during the growing season (May to September) to avoid the dilution effect of non-growing season periods (e.g., winter snow cover) on sensitivity estimates. We use the 16-day MODIS_ NDVI data as an indicator of vegetation growth status and employ climate driving factors from the National Tibetan Plateau Scientific Data Center, including temperature, cumulative precipitation, and solar radiation. These factors are matched with the corresponding dates of the 16-day NDVI data. A pixel-level time series dataset covering the growing seasons from 2000 to 2023 is then constructed, reflecting the vegetation's dynamic growth response characteristics in the high-elevation, high-radiation, and low-temperature environment of the Tibetan Plateau.

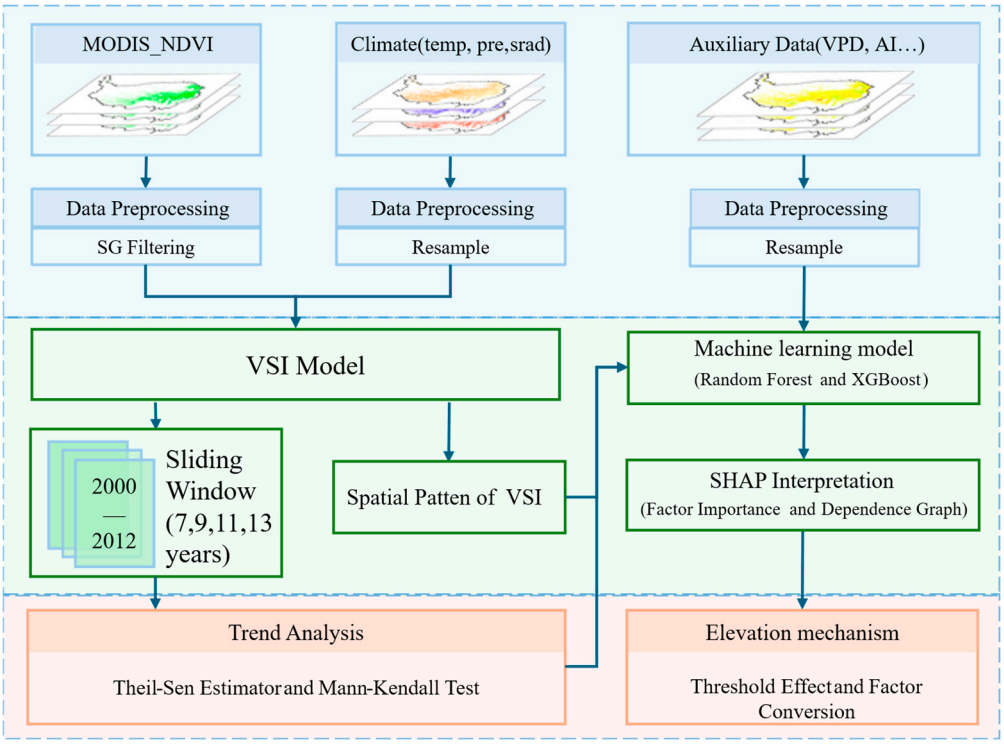


Figure 2. Technical flowchart, where temp refers to temperature, pre refers to cumulative precipitation, srad refers to solar radiation, VPD refers to vapor pressure deficit, AI refers to Aridity Index, and VSI refers to Vegetation Sensitivity Index.

2.3.1. Calculation of Vegetation Sensitivity Index

To analyze the potential impact of memory effects on vegetation growth on the Tibetan Plateau, this study introduces the lagged NDVI anomaly from two 16-day periods (NDVIt-2) as a fourth variable. To ensure that the collinearity among climate variables does not affect the estimation, we include temperature, cumulative precipitation, solar radiation, and NDVIt-2 in Principal Component Analysis to extract the response principal

components (PCs). Following the method of Seddon et al. [6], we apply PCR to regress the standardized NDVI anomalies onto the extracted PCs. After testing the significance of the PCR coefficients at the pixel level, we apply a hierarchical threshold strategy; a strict level of ($p < 0.05$) is used for the full-period analysis to ensure robustness, while the threshold is adjusted to ($p < 0.1$) for the dynamic analysis to mitigate the risk of false negatives associated with reduced statistical power in shorter time series. We then back-project the results onto the original variable scale using the principal component loadings. This yields the standardized regression coefficients for temperature, cumulative precipitation, solar radiation, and NDVIt-2 (denoted as $\alpha(i)$, $\beta(i)$, $\gamma(i)$, and $\lambda(i)$, respectively). The regression model is

$$\mathrm{NDVI}_t = \alpha \cdot \mathrm{Tem}_t + \beta \cdot \mathrm{Prec}_t + \gamma \cdot \mathrm{Rad}_t + \lambda \cdot \mathrm{NDVI}_{t-2} + \varepsilon \quad (1)$$

where λ captures the vegetation's sustained response to the previous composite period's state, and ε represents the residual error.

For the PCs with significant coefficients, the cumulative sum of the product of their loadings and regression coefficients is used to back-calculate the combined impact of the original variables on NDVI.

$$\mathrm{VSI} = \alpha \cdot \mathrm{SI_Tem} + \beta \cdot \mathrm{SI_Prec} + \gamma \cdot \mathrm{SI_Rad} \quad (2)$$

where SI_Tem, SI_Prec, and SI_Rad represent the native sensitivity indices of the ecosystem to temperature, cumulative precipitation, and solar radiation, respectively.

The VSI is then obtained by summing the absolute values of all standardized coefficients. Both the VSI and the coefficients α, β, γ, and λ are standardized using min-max normalization to a range of 0–100. It is worth noting that the lag term (λ) was included in the regression model solely to separate climate effects from ecological memory. However, it was explicitly excluded from the VSI calculation because the VSI aims to quantify an ecosystem's sensitivity to external climate variability, not its internal biotic persistence [6].

2.3.2. Trend Analysis

To reveal the temporal dynamics of the VSI, this study introduced a 13-year sliding time window based on the entire period (2000–2023). The selection of this specific window size was supported by a sensitivity analysis conducted in this study (comparing lengths of 7, 9, 11, and 13 years), which demonstrated that VSI spatial patterns remained highly robust and consistent across all scales. Ultimately, we selected the 13-year duration to maximize the number of regression observations, thereby enhancing the statistical stability of the sensitivity coefficients and effectively suppressing the interference of short-term interannual noise. Consequently, continuous subsequences were generated with a one-year step (e.g., 2000–2012, 2001–2013, …, 2011–2023). For each subsequence, the VSI was calculated using the same method as for the entire period. The temporal trend of each window's VSI was then quantified using Theil-Sen median trend analysis [39], and the significance of the trend was verified using the Mann–Kendall test [40] ($p < 0.05$). The Theil-Sen median trend analysis is a robust non-parametric statistical method used to describe trends in long-term datasets. The calculation formula is as follows:

$$\mathrm{Slope} = \mathrm{Median}\left(\frac{X_j - X_i}{j - i}\right), i < j \leq n \quad (3)$$

where Slope is the slope, and i and j are the end years of the corresponding time window, i.e., i, j = 2012, 2013, …, n, n = 2023. X_i and X_j represent the target data at time steps i and j, respectively. A positive value of Slope indicates that the target dataset is on an upward trend, and a negative value indicates that the target dataset is on a downward trend.

To verify robustness, this study compared VSI change patterns under different time windows (7, 9, 11, 13 years) to capture the phased changes and potential scale dependence of vegetation sensitivity.

2.3.3. Attribution Analysis of Sensitivity Trends

To attribute the driving factors behind the VSI trends, this study employed machine learning models combined with Shapley Additive exPlanations (SHAP) for interpretability. All analyses were conducted using Python (version 3.8) with the scikit-learn and xgboost libraries for model implementation, and the shap library for SHAP value calculation and visualization. Specifically, eXtreme Gradient Boosting (XGBoost) and RF ensemble models are used, with the VSI trend slope as the response variable and input factors including natural and human activity factors. These models can separate the marginal contributions of each predictor to the target variable. The RF model reduces variance by constructing multiple independent learners based on the bootstrap aggregating strategy [41]. The XGBoost model, on the other hand, reduces bias by constructing strong and mutually dependent estimators using the boosting tree strategy [42]. To ensure model reproducibility and robustness, we implemented a rigorous 'coarse-to-fine' two-stage hyperparameter optimization strategy for both models, rather than relying on default configurations. The dataset was partitioned into training (80%), validation (10%), and independent testing (10%) subsets. We first conducted a Randomized Search with 5-fold cross-validation to identify promising hyperparameter regions, followed by a refined Grid Search to precisely locate the global optima. Final model performance was evaluated on the independent testing set. SHAP values are used to quantify the relative importance and directional influence of each factor on VSI trends, outputting global importance rankings and local interpretation plots to reveal the regulatory mechanisms of gradient effects such as elevation.

3. Results

3.1. Spatial Distribution Pattern of Vegetation Sensitivity on the Tibetan Plateau

The spatial distribution of the VSI on the Tibetan Plateau from 2000 to 2023 exhibits significant spatial variation (Figure 3), with generally higher vegetation sensitivity in the southern and central-southern regions. Among these, the sensitivity in the southwestern IC2 eco-zone is the highest, followed by IIAB1eco-zone and the eastern part of IB1 eco-zone. In these areas, the alpine vegetation's sensitivity to climate is significantly higher than the plateau's average level of 22.86. In contrast, the northern regions show lower vegetation sensitivity to climate change. Specifically, IIC1eco-zone has the lowest sensitivity, followed by IID1eco-zone and IID2 eco-zone, with the eastern part of IC1 eco-zone also showing lower VSI. These results indicate that the vegetation sensitivity to climate change on the Tibetan Plateau generally follows a spatial pattern that is higher in the southwest and lower in the northeast.

From 2000 to 2023, the sensitivity of alpine vegetation to precipitation, solar radiation, and temperature exhibits notable spatial variation (Figure 4). Specifically, regarding sensitivity to precipitation, the southwestern region shows relatively higher sensitivity, especially in the central and western parts of IC2 eco-zone, indicating that vegetation growth in these areas is primarily water-limited. High-radiation-sensitivity areas are concentrated in the central plateau, with the northern part of IC2 eco-zone, southwestern IC1 eco-zone, and the western part of IB1 eco-zone forming the high-value zone. High-temperature sensitivity areas are located in the southern part of the Tibetan Plateau, while vegetation in the northern plateau shows relatively low sensitivity to temperature. These results demonstrate that the southwest—high, northeast—low spatial pattern of the VSI on the Tibetan Plateau is driven by the spatial differences in dominant climate-limiting factors.

Specifically, the southwestern region is limited by both precipitation and temperature, the central region is primarily limited by radiation, and the northern region shows relatively low sensitivity to all climate factors.

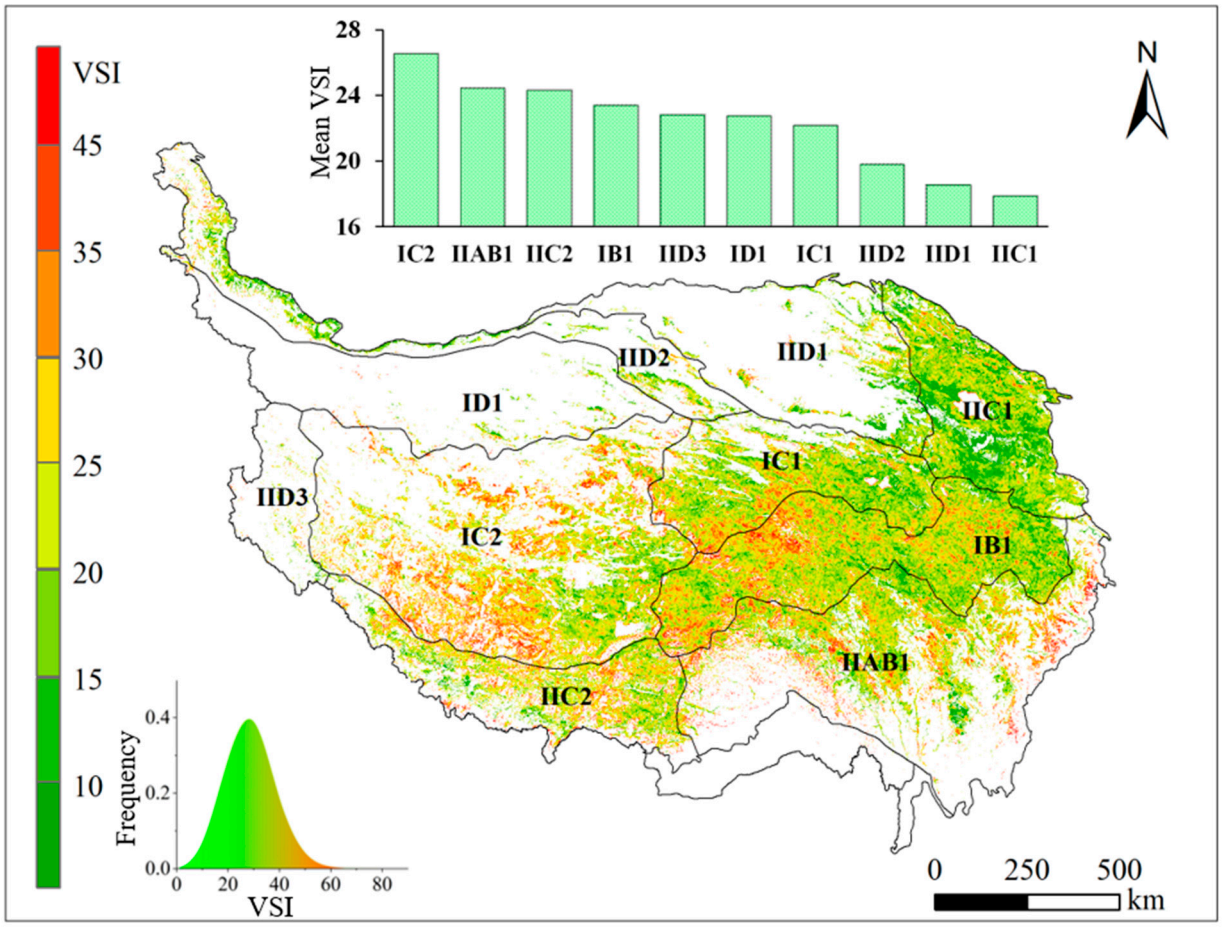


Figure 3. Spatial distribution of the Vegetation Sensitivity Index (VSI) on the Tibetan Plateau during 2000–2023. The subplot in the lower-left corner indicates the frequency distribution of the VSI, while the bar chart in the top denotes the mean VSI of each eco-zone.

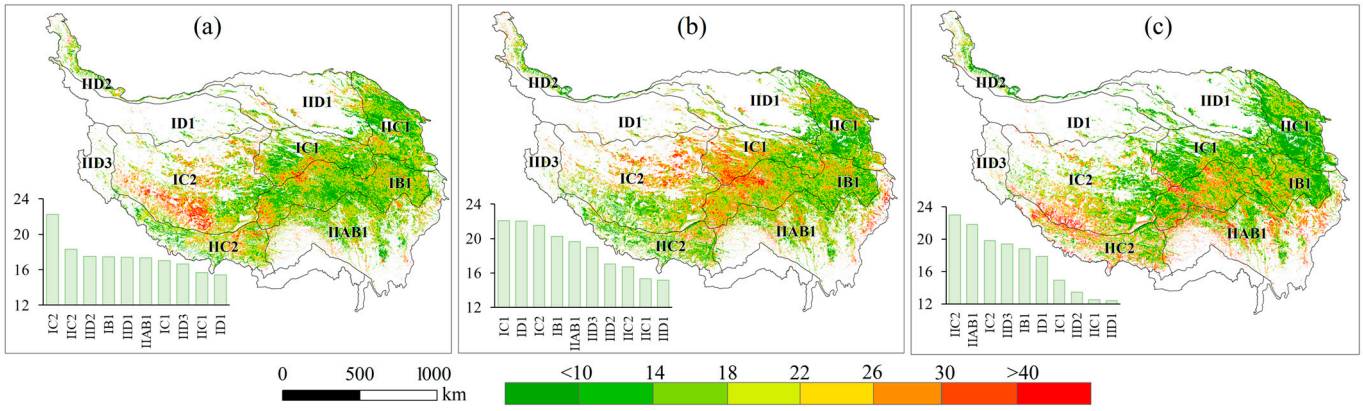


Figure 4. Spatial patterns of vegetation sensitivity to different climate factors on the Tibetan Plateau. (**a**–**c**) denote the spatial distribution of vegetation sensitivity to precipitation, radiation, and temperature, respectively.

3.2. Spatiotemporal Change in Vegetation Sensitivity on the Tibetan Plateau

The VSI change patterns under different sliding windows (7, 9, 11, 13 years) show high consistency (Figure S1), and all exhibit a phased fluctuation and upward trend, which confirms the robustness of the analysis results. Using a 13-year sliding window (from 2000–2012 to 2011–2023) as an example, we further characterize the spatiotemporal evolution of the VSI across the Tibetan Plateau from 2000 to 2023 (Figure 5). Among the vegetation pixels, 56.31% show an increasing trend in the VSI, while 43.69% show a decreasing trend. The areas with significant VSI increases are concentrated in the northern regions, including ID1, IID1, IC1, and IID2 eco-zones. In contrast, although the overall sensitivity of the plateau shows an upward trend, the decreasing trend in the VSI exhibits clear spatial clustering, mainly in the southern and southeastern regions, including IIAB1, IIC2, and IC2. The IIC1 in the northeastern region shows a weak increase or remains relatively stable.

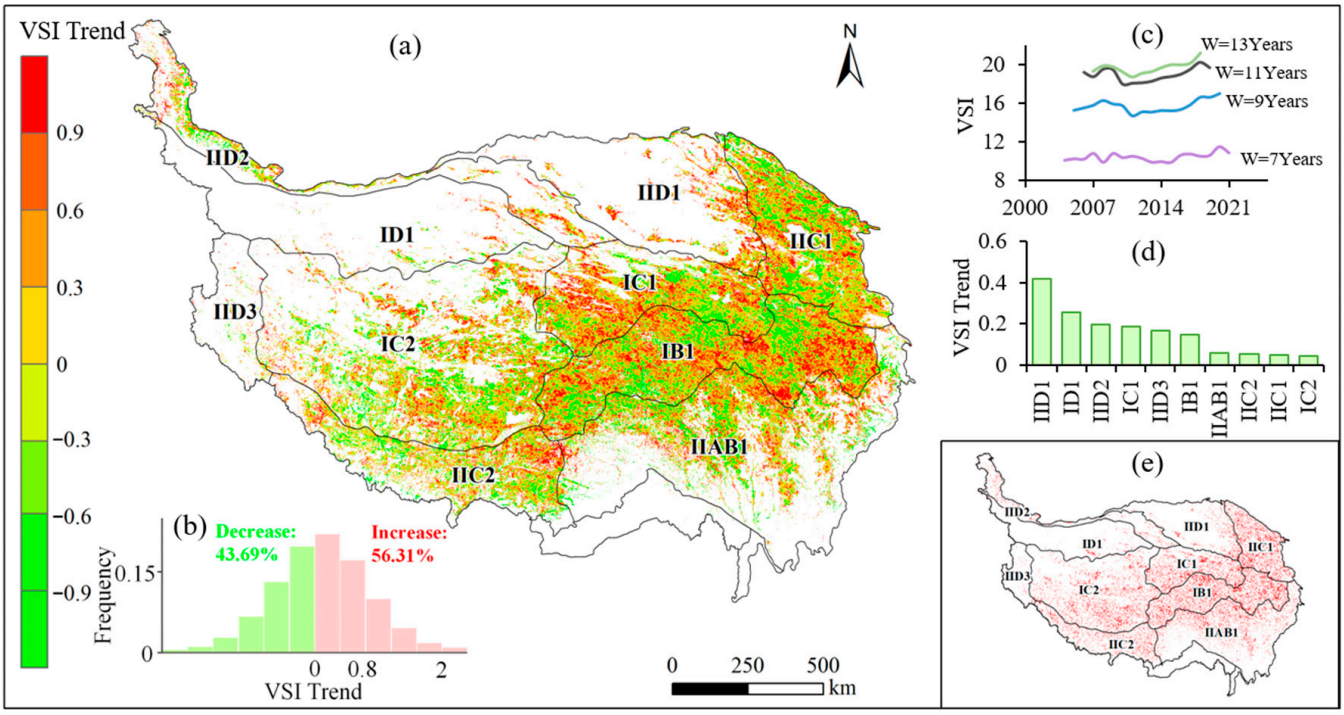


Figure 5. Spatiotemporal change in the Vegetation Sensitivity Index (VSI) on the Tibetan Plateau during 2000–2023. (**a**) Spatial pattern of the change in the VSI; (**b**) frequency distribution of the change in the VSI; (**c**) temporal variation in the VSI under different moving window widths; (**d**) mean VSI trend in each eco-zone across the Tibetan Plateau; and (**e**) spatial distribution of statistical significance ($p < 0.05$).

The spatial distribution and zonal statistics of the sensitivity change trend in vegetation on the Tibetan Plateau to different climate factors reveal the spatiotemporal dynamic differences in vegetation response sensitivity to precipitation, radiation, and temperature (Figure 6). Specifically, the areas with high precipitation sensitivity change trends are concentrated in the northern desert regions of the Tibetan Plateau, such as IID1 eco-zone and IID3 eco-zone. In contrast, large negative value areas are observed in the southern and central-southern alpine meadow and grassland regions, such as IIC2 eco-zone. High radiation sensitivity change trends are found in the central and northeastern grassland areas, such as the eastern part of IC2 and IC1 eco-zones, while the southern regions, like IIC2 eco-zone, show predominantly negative values. The sensitivity change trends in vegetation to temperature in the northern plateau exhibit an overall slight positive trend, but large negative values are observed in the central regions, including IC2, IC1, and IB1

eco-zones. Overall, the sensitivity change trends in vegetation to climate factors show spatial heterogeneity across different ecological regions of the Tibetan Plateau.

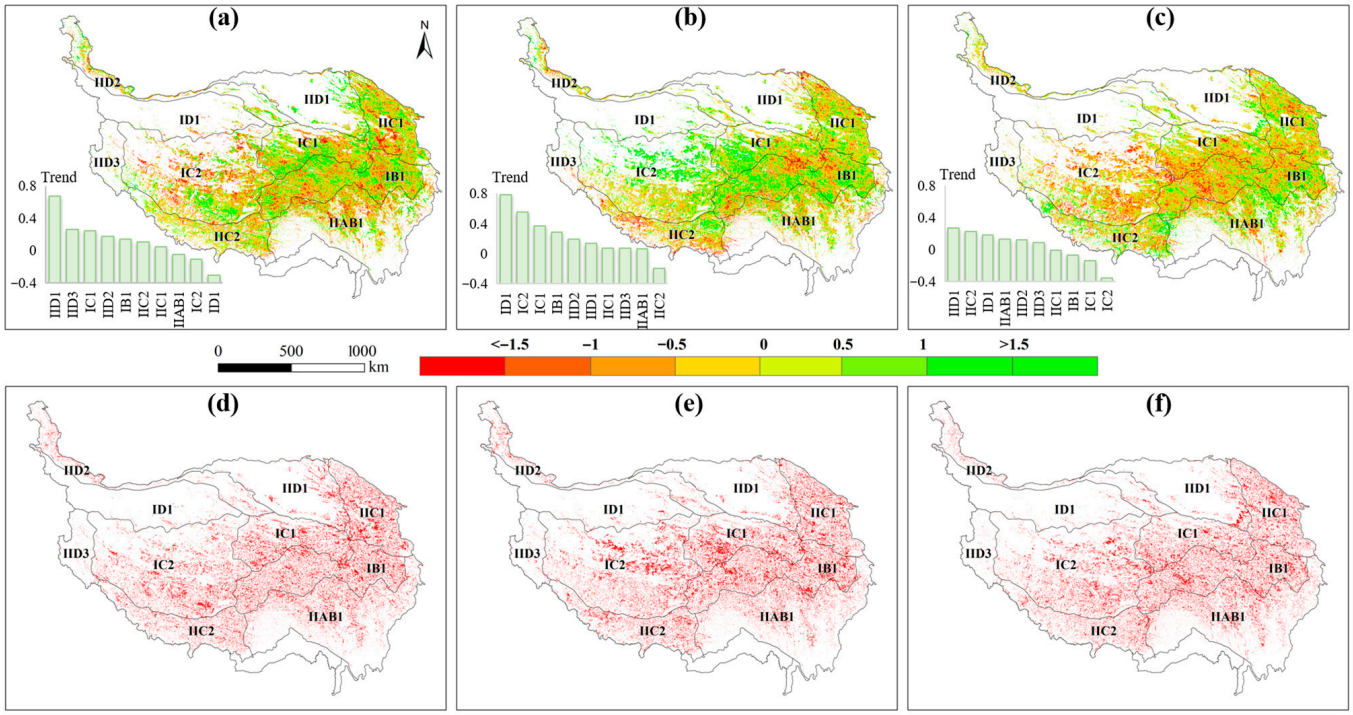


Figure 6. Spatial distribution of vegetation sensitivity change trend to key climate factors on the Tibetan Plateau. (**a**–**c**) Spatial pattern of vegetation sensitivity change trend to precipitation, radiation, and temperature, respectively. (**d**–**f**) Corresponding spatial distributions of areas with statistically significant ($p < 0.05$) vegetation sensitivity change trends for precipitation, radiation, and temperature, respectively.

3.3. Attribution of Vegetation Sensitivity Trends on the Tibetan Plateau

We applied the SHAP algorithm to the XGBoost and RF models to identify the factors with relative importance in driving the observed trends in the VSI on the Tibetan Plateau. The relative importance rankings of multiple driving factors in both models are highly consistent (Figure 7), indicating that elevation is the most dominant factor shaping the spatial pattern of vegetation sensitivity, with its relative importance far exceeding other natural factors such as temperature, solar radiation, and precipitation, while the impact of human activities is the weakest. Further SHAP dependence plots reveal the nonlinear regulatory characteristics of elevation on the VSI; elevation is significantly positively correlated with SHAP values ($R = 0.96$), but there is a clear threshold effect (Figure 8). Below an elevation of approximately 4500 m, the contribution of elevation to sensitivity remains in a low negative range and changes steadily. However, when the elevation exceeds 4500 m, the SHAP values increase sharply and linearly with elevation, indicating that high-elevation environmental characteristics have a significant and rapidly enhancing positive contribution to vegetation sensitivity.

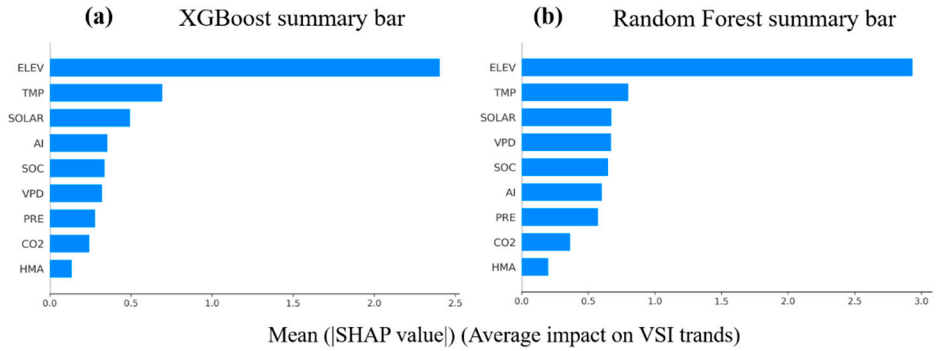


Figure 7. Relative importance ranking of trend-driving factors for vegetation sensitivity based on Shapley Additive exPlanations (SHAP) values. (**a**) eXtreme Gradient Boosting (XGBoost) model results; (**b**) Random Forest (RF) model results. ELEV refers to elevation, temp refers to temperature, SOLAR refers to solar radiation, AI refers to Aridity Index, SOC refers to soil organic carbon, VPD refers to vapor pressure deficit, PRE refers to precipitation, CO_2 refers to carbon dioxide, and HMA refers to human activity.

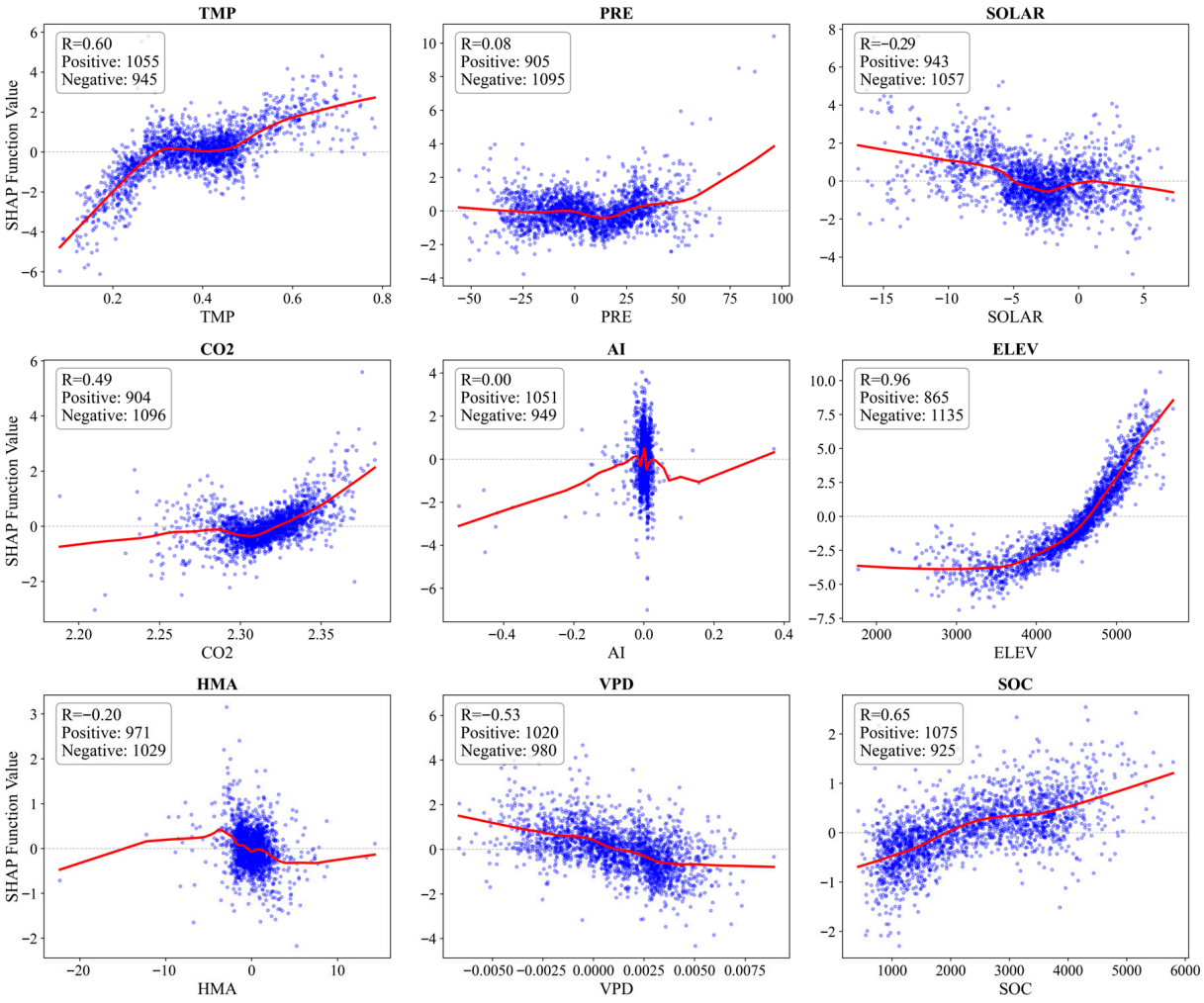


Figure 8. Nonlinear responses and threshold effects of vegetation sensitivity drivers on the Tibetan Plateau based on Shapley Additive exPlanations (SHAP) dependency graphs. TMP denotes temperature; PRE denotes precipitation; SOLAR denotes solar radiation; CO_2 denotes carbon dioxide; AI denotes aridity index; ELEV denotes elevation; HMA denotes human activity intensity; VPD denotes vapor pressure deficit; SOC denotes soil organic carbon.

3.4. Regulatory Effect of Elevation on Vegetation Sensitivity

To explore the gradient regulatory effect of elevation on the VSI, this study analyzed the mean values and linear trends in the VSI across different elevation intervals during the entire study period. Furthermore, based on 12 sliding windows of 13 years (from 2000–2012 to 2011–2023), we analyzed the long-term change trends in the VSI in each elevation interval. The results show that the VSI increases significantly with elevation ($R^2 = 0.93$, $p < 0.001$), indicating that, under the current climate conditions, vegetation at higher elevation responds more strongly to climate variability than vegetation at lower elevation (Figure 9a). However, the long-term trend in VSI change slows significantly with increasing elevation (Figure 9b). In relatively lower elevation regions (<4600 m), the VSI shows the fastest growth trend, while in high-elevation regions (>5000 m), this growth trend gradually slows down with increasing elevation, and even becomes negative in extremely high-elevation areas. These results suggest that during the period of 2000–2023, the impacts of climate variability on low-elevation ecosystems is accelerating, while, despite the highest baseline sensitivity in high-elevation ecosystems, their sensitivity has not significantly increased further.

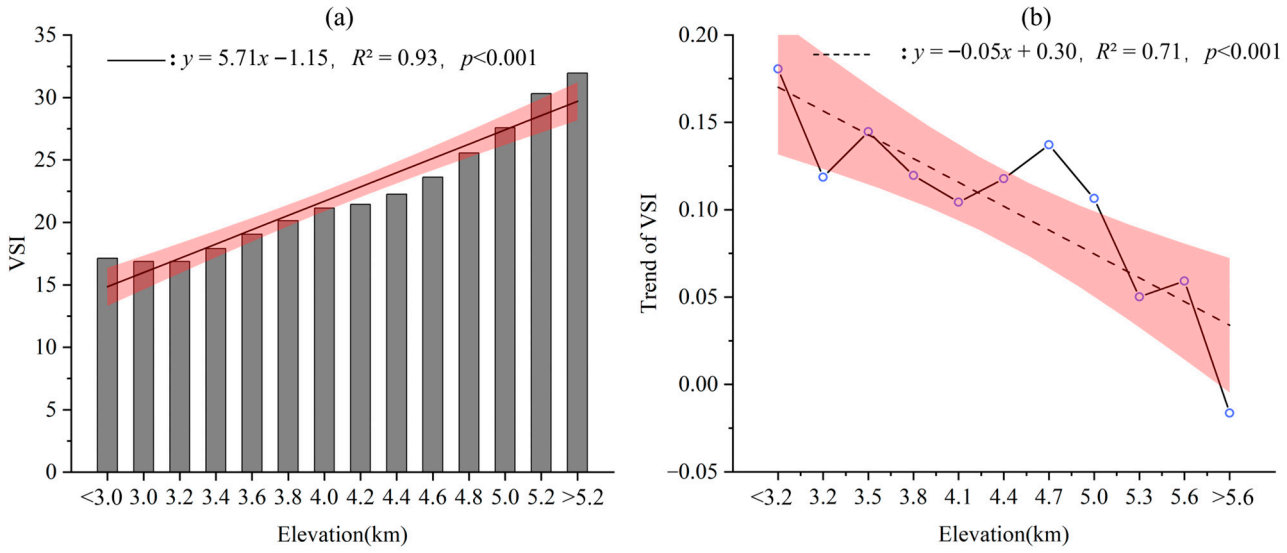


Figure 9. The regulatory effect of elevation on vegetation sensitivity and its change trends. (**a**) Variation in the mean Vegetation Sensitivity Index (VSI) along the elevation gradient; (**b**) variation in the VSI change trend along the elevation gradient. The black lines represent the linear regression fits, and the red shaded areas indicate the 95% confidence bands.

To further reveal the driving mechanisms of the aforementioned elevation-based differentiation of the VSI, this study analyzes the variation characteristics of temperature, radiation, and precipitation sensitivity with elevation, as well as their dynamic evolution based on 12 sliding windows of 13 years (Figure 10). The results show that sensitivity to all three factors increases significantly with elevation, with temperature sensitivity showing the greatest increase (slope = 7.31, $R^2 = 0.88$, $p < 0.001$), much higher than radiation (slope = 3.51) and precipitation (slope = 2.36). This indicates that as elevation increases, vegetation's response to temperature variation is the strongest, serving as the core driver for the rapid rise in the VSI with elevation. However, in terms of long-term trends, the trend of change in temperature sensitivity is close to zero at lower elevations and decreases sharply to significant negative values above 4700 m. In contrast, radiation sensitivity shows a clear increasing trend across all elevation intervals, with this trend being especially pronounced in the middle- to high-elevation regions. This suggests that, although high-elevation vegetation is currently the most sensitive to temperature, its sensitivity is rapidly

weakening, while its sensitivity to radiation has continuously and significantly increased over the past 20 years.

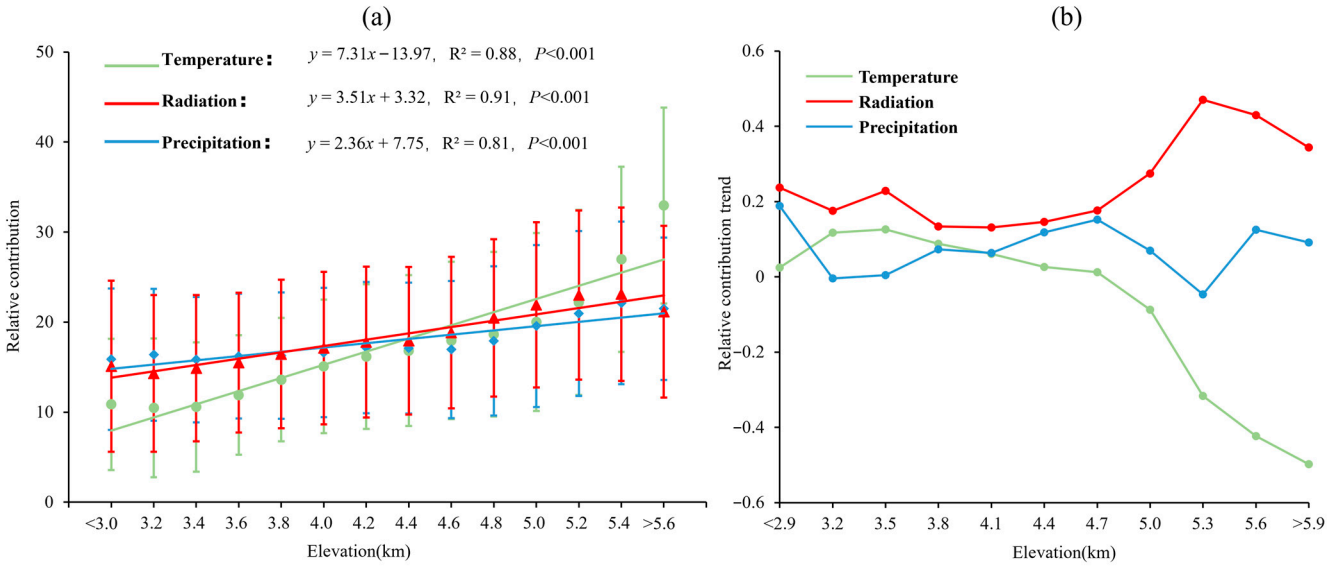


Figure 10. The distribution characteristics of vegetation sensitivity to different climate factors and their change trends along the elevation gradient. (**a**) Variation in sensitivity to the three factors with elevation; (**b**) variation in the change trends of sensitivity to the three factors with elevation.

4. Discussion

4.1. Ecological Mechanisms of Spatial Patterns of the VSI for Alpine Grasslands

This study reveals a significant spatial pattern of the VSI on the Tibetan Plateau, with a higher in the southwest, lower in the northeast distribution (Figure 3). This result is highly consistent with previous research based on data from 2000 to 2016 [6]. Although this study extends the observation period to 2023, covering a longer span of climate variability, the spatial differentiation of vegetation sensitivity remains stable. The high consistency across different time periods not only strongly validates the reliability of this study's data but also supports and refines the ecosystem sensitivity framework proposed by Seddon et al. [6] on a global scale, which suggests that ecosystem vulnerability mainly depends on the critical state of its limiting factors.

In northern desert regions, lower VSI values reflect the evolutionary adaptations of drought-tolerant species, which may have developed robust biological buffering mechanisms to withstand prolonged environmental stress. Desert vegetation remains in a dormant or low-metabolism state for extended periods, developing tolerance to extreme conditions [43]. By reducing metabolic trends and forming adaptive structures (e.g., deep root systems, thick cuticles), it buffers the impacts of climate variability [44], leading to lower sensitivity. Additionally, this study finds that vegetation in the central regions of the Tibetan Plateau is primarily radiation-limited, which may reflect the compounded effects of light suppression or intensified evapotranspiration under high-radiation conditions [45].

4.2. Evolution of the VSI for Alpine Grasslands

From 2000 to 2023, the VSI on the Tibetan Plateau showed an overall increasing trend in time and space. The increase in the northeastern region was significantly greater than in the southwestern region, and large areas of VSI decline appeared in the southwest, deeply reflecting the ecosystem's response to the plateau's climatic transition. A large body of observational evidence indicates that the Tibetan Plateau has experienced a pronounced warming and wetting process over the past decades, with a warming rate approximately

twice the global average [24,46–48]. In the northern and northwestern parts of the plateau, the significant rise in the VSI indicates that vegetation stability in these areas is declining, shifting from a relatively stable adaptive state to a less stable state that is more susceptible to climatic disturbances. This suggests that under the warming-and-wetting background, increased water availability may be altering the region's ecological constraint thresholds. Although increased precipitation has enhanced desert vegetation cover, the resulting expansion also increases water demand, potentially making the ecosystem more sensitive to precipitation variability [49].

In contrast, the decline in the VSI in the alpine meadow and shrub areas of the central-southern Tibetan Plateau suggests the vegetation's "thermal adaptation" and enhanced resilience. With the extension of the growing season and the increase in accumulated temperature, vegetation in the southern regions has gradually reduced its sensitivity to temperature fluctuations through phenological adjustments and physiological adaptations [7]. This phenomenon aligns with the trend in weakened temperature sensitivity observed by Piao et al. [50] in the Northern Hemisphere. However, it is noteworthy that Wu et al. [51] pointed out that, over a longer timescale (1982-2015), forests and grasslands in the southeastern region have shown an increasing trend in sensitivity. This discrepancy may stem from differences in observation periods and the ability of remote sensing data sources to capture vegetation signals. Meanwhile, the increased radiation sensitivity of vegetation in the central plateau and some high-elevation areas reflects a shift in limiting factors. As the warming and wetting trend has significantly alleviated the region's harsh moisture and low-temperature constraints, radiation is gradually replacing water–energy factors as the new bottleneck limiting vegetation growth.

4.3. Elevation Gradient Regulation of the VSI for Alpine Grasslands on the Tibetan Plateau

This study revealed that elevation is the core factor driving the evolution of the VSI on the Tibetan Plateau. Different elevation intervals exhibit a vertical differentiation pattern of "high elevation, high vulnerability, low growth" and "low elevation, low vulnerability, high growth". Specifically, the VSI increases significantly with elevation, indicating that high-elevation regions are highly sensitive areas of ecological vulnerability on the plateau. The high-elevation regions of the Tibetan Plateau are typical "climate-limited systems", where the marginal effects of vegetation growth are highly controlled by heat or temperature [52]. This single dominant factor control mechanism prevents any compensatory interactions between factors, leading to higher sensitivity to temperature fluctuations. Crucially, our analysis identifies a distinct non-linear surge in sensitivity at approximately 4700 m. This threshold likely results from the superposition of ecological and climatic transitions [13,53–55]. However, in terms of the evolution trend, the rate of sensitivity increase in high-elevation areas is significantly slower than in low-elevation areas, due to the heat-buffering effect brought about by "elevation-dependent warming" [53]. Intense warming has brought high-elevation habitats' temperatures closer to the physiological optimum for vegetation [56], partially offsetting the pressure from increased resource demand. Vegetation in low-elevation areas appears to be shifting from 'temperature-dominated' to 'water-limited' regimes, potentially facing a heightened risk of degradation compared to vegetation at higher elevations.

4.4. Limitations and Future Work

Although this study reveals the spatiotemporal evolution characteristics of vegetation sensitivity to climate change on the Tibetan Plateau, there are still some limitations. Precipitation does not fully equate to the soil moisture available to vegetation. On the Tibetan Plateau, processes like the melting of permafrost and snowmelt alter the soil water and

heat transfer mechanisms. Considering only atmospheric precipitation may lead to biased assessments of the water-limiting effect [52,57]. Furthermore, this study has not explicitly integrated the fertilization effect of increasing atmospheric CO_2 concentration. The rise in CO_2 concentration typically enhances vegetation's water use efficiency, which could partially alleviate drought stress induced by climate warming. Ignoring this factor may lead to uncertainties on identifying vegetation sensitivity due to climate change. In addition, vegetation's response to climate change exhibits ecological memory effects, and the nonlinear regulatory effects of human activities on sensitivity still need further refinement [6,58]. Moreover, while this study focuses on climate drivers, grazing and ecological engineering (e.g., grassland restoration) have profoundly altered the community structure and resilience of alpine grasslands. For instance, moderate grazing can increase ecosystem resilience, while overgrazing exacerbates vulnerability [59–61]. Future research should attempt to develop integrated assessment models that couple "natural-social" systems to quantify the extent to which human activities offset or amplify the risks of climate change [62,63].

5. Conclusions

This study elucidates the spatiotemporal response characteristics of the Tibetan Plateau's alpine grasslands to climate change through the construction of a dynamic VSI framework. The results showed that the VSI of alpine vegetation follows a higher in the southwest, lower in the northeast spatial pattern. Under the ongoing warming and wetting climate trend, the VSI exhibits an overall increasing trend. However, the dominant climate factors in different regions have diverged; sensitivity to precipitation has generally increased in the northern and northwestern desert areas, sensitivity to temperature has decreased in the southern alpine meadow and shrub areas, and sensitivity to solar radiation has increased in the central and some high-elevation areas. Attribution analysis further reveals that elevation is a key environmental factor controlling this spatial pattern and its evolution trend, showing a nonlinear regulatory characteristic of higher sensitivity at higher elevations, with lower growth rates. These findings help clarify the dynamic evolution mechanisms of alpine ecosystem sensitivity and provide scientific support for the development of differentiated ecological management strategies.

Supplementary Materials: The following supporting information can be downloaded at https://www.mdpi.com/article/10.3390/land15020215/s1, Figure S1: Spatial distribution of mean vegetation sensitivity index (VSI) on the Tibetan Plateau under different moving time windows; Figure S2: Correlation Matrix Plot of All Variables; Table S1: Overall and Factor-Specific Average Vegetation Sensitivity Index (VSI) Across Different Ecosystem Zones of the Qinghai-Tibet Plateau (2000–2023); Table S2: Temporal trends in overall vegetation sensitivity index (VSI) and average VSI for different factors across various ecosystem zones of the Tibetan Plateau (2000–2023).

Author Contributions: Conceptualization, Z.X. and L.L.; methodology, Z.X. and B.Z.; formal analysis, S.F. and Y.L.; data curation, B.Z., Z.X. and L.L.; writing—original draft preparation, Z.X., W.L., L.L. and S.F.; writing—review and editing, H.L., X.Z. and F.D.; visualization, Z.X.; supervision, F.D.; funding acquisition, L.L. and W.L. All authors have read and agreed to the published version of the manuscript.

Funding: This research was funded by the National Science Foundation of China (Grant No. 42101099) and Natural Science Foundation of Fujian Province (Grant No. 2023J011425).

Data Availability Statement: Data are contained within this article or its Supplementary Materials. Further inquiries can be directed to the corresponding authors.

Conflicts of Interest: The authors declare no conflicts of interest.

Abbreviations

The following abbreviations are used in this manuscript:

VSI	Vegetation Sensitivity Index
RF	Random Forest
XGBoost	eXtreme Gradient Boosting
SHAP	Shapley Additive exPlanations
PCR	Principal Component Regression
IIAB1	The temperate humid/sub-humid western Sichuan–eastern Tibet montane coniferous forest zone
IB1	sub-cold sub-humid Guoluo-Naqu mountain alpine shrub-meadow zone
IIC2	temperate semi-arid eastern Qinghai-Qilian montane steppe zone
IC1	sub-cold semi-arid southern Qinghai alpine meadow-steppe
IC2	Qiangtang alpine steppe zones
IIC1	Temperate semi-arid southern Tibet montane shrub-steppe zone
IID2	Temperate arid Qaidam Basin desert region
IID3	Temperate arid north Kunlun desert zone
ID1	Sub-cold arid Kunlun mountain and plateau alpine steppe zone
IID1	Temperate arid Ngali montane desert zone

References

1. Piao, S.; Cui, M.; Chen, A.; Wang, X.; Ciais, P.; Liu, J.; Tang, Y. Altitude and temperature dependence of change in the spring vegetation green-up date from 1982 to 2006 in the Qinghai-Xizang Plateau. *Agric. For. Meteorol.* **2011**, *151*, 1599–1608. [CrossRef]
2. Zhang, Y.L.; Li, L.H.; Ding, M.J.; Zheng, D. Greening of the Tibetan Plateau and its drivers since 2000. *Chin. J. Nat.* **2017**, *39*, 173–178.
3. Ma, Y.; Zhong, L.; Jia, L.; Menenti, M. Land–Atmosphere Interactions and Effects on the Climate of the Tibetan Plateau and Surrounding Regions II. *Remote Sens.* **2023**, *15*, 4540. [CrossRef]
4. Huang, J.; Zhou, X.; Wu, G.; Xu, X.; Zhao, Q.; Liu, Y.; Duan, A.; Xie, Y.; Ma, Y.; Zhao, P.; et al. Global Climate Impacts of Land-Surface and Atmospheric Processes Over the Tibetan Plateau. *Rev. Geophys.* **2023**, *61*, e2022RG000771. [CrossRef]
5. Boone, R.B.; Conant, R.T.; Sircely, J.; Thornton, P.K.; Herrero, M. Climate change impacts on selected global rangeland ecosystem services. *Glob. Change Biol.* **2018**, *24*, 1382–1393. [CrossRef] [PubMed]
6. Seddon, A.W.R.; Macias-Fauria, M.; Long, P.R.; Benz, D.; Willis, K.J. Sensitivity of global terrestrial ecosystems to climate variability. *Nature* **2016**, *531*, 229–232. [CrossRef] [PubMed]
7. Shen, M.; Wang, S.; Jiang, N.; Sun, J.; Cao, R.; Ling, X.; Fang, B.; Zhang, L.; Zhang, L.; Xu, X.; et al. Plant phenology changes and drivers on the Qinghai–Tibetan Plateau. *Nat. Rev. Earth Environ.* **2022**, *3*, 633–651. [CrossRef]
8. Lehnert, L.W.; Wesche, K.; Trachte, K.; Reudenbach, C.; Bendix, J. Climate variability rather than overstocking causes recent large scale cover changes of Tibetan pastures. *Sci. Rep.* **2016**, *6*, 24367. [CrossRef]
9. Piao, S.; Fang, J.; He, J. Variations in Vegetation Net Primary Production in the Qinghai-Xizang Plateau, China, from 1982 to 1999. *Clim. Change* **2006**, *74*, 253–267. [CrossRef]
10. Chen, Z.; Liu, H.; Xu, C.; Wu, X.; Liang, B.; Cao, J.; Chen, D. Modeling vegetation greenness and its climate sensitivity with deep-learning technology. *Ecol. Evol.* **2021**, *11*, 7335–7345. [CrossRef]
11. Forzieri, G.; Girardello, M.; Ceccherini, G.; Spinoni, J.; Feyen, L.; Hartmann, H.; Beck, P.S.A.; Camps-Valls, G.; Chirici, G.; Mauri, A.; et al. Emergent vulnerability to climate-driven disturbances in European forests. *Nat. Commun.* **2021**, *12*, 1081. [CrossRef]
12. Myers-Smith, I.H.; Kerby, J.T.; Phoenix, G.K.; Bjerke, J.W.; Epstein, H.E.; Assmann, J.J.; John, C.; Andreu-Hayles, L.; Angers-Blondin, S.; Beck, P.S.A.; et al. Complexity revealed in the greening of the Arctic. *Nat. Clim. Change* **2020**, *10*, 106–117. [CrossRef]
13. Li, L.; Zhang, Y.; Wu, J.; Li, S.; Zhang, B.; Zu, J.; Zhang, H.; Ding, M.; Paudel, B. Increasing sensitivity of alpine grasslands to climate variability along an elevational gradient on the Qinghai-Tibet Plateau. *Sci. Total Environ.* **2019**, *678*, 21–29. [CrossRef] [PubMed]
14. Luo, M.; Wu, S.; Lau, G.N.; Pei, T.; Liu, Z.; Wang, X.; Ning, G.; Chan, T.O.; Yang, Y.; Zhang, W. Anthropogenic forcing has increased the risk of longer-traveling and slower-moving large contiguous heatwaves. *Sci. Adv.* **2024**, *10*, eadl1598. [CrossRef]
15. van Westen, R.M.; Kliphuis, M.; Dijkstra, H.A. Physics-based early warning signal shows that AMOC is on tipping course. *Sci. Adv.* **2024**, *10*, eadk1189. [CrossRef]
16. Zhang, W.; Zhou, T.; Wu, P. Anthropogenic Amplification of Precipitation Variability over the Past Century. *Science* **2024**, *385*, 427–432. [CrossRef]

17. Yin, J.; Gentine, P.; Slater, L.; Gu, L.; Pokhrel, Y.; Hanasaki, N.; Guo, S.; Xiong, L.; Schlenker, W. Future Socio-Ecosystem Productivity Threatened by Compound Drought–heatwave Events. *Nat. Sustain.* **2023**, *6*, 259–272. [CrossRef]
18. Piao, S.; Wang, X.; Park, T.; Chen, C.; Lian, X.; He, Y.; Bjerke, J.W.; Chen, A.; Ciais, P.; Tømmervik, H.; et al. Characteristics, drivers and feedbacks of global greening. *Nat. Rev. Earth Environ.* **2020**, *1*, 14–27. [CrossRef]
19. Reichstein, M.; Bahn, M.; Ciais, P.; Frank, D.; Mahecha, M.D.; Seneviratne, S.I.; Zscheischler, J.; Beer, C.; Buchmann, N.; Frank, D.C.; et al. Climate extremes and the carbon cycle. *Nature* **2013**, *500*, 287–295. [CrossRef]
20. Chen, J.; Yang, H.; Jin, T.; Wu, K. Assessment of terrestrial ecosystem sensitivity to climate change in arid, semi-arid, sub-humid, and humid regions using EVI, LAI, and SIF products. *Ecol. Indic.* **2024**, *158*, 111511. [CrossRef]
21. Zhang, Y.; Gentine, P.; Luo, X.; Lian, X.; Liu, Y.; Zhou, S.; Michalak, A.M.; Sun, W.; Fisher, J.B.; Piao, S.; et al. Increasing sensitivity of dryland vegetation greenness to precipitation due to rising atmospheric CO_2. *Nat. Commun.* **2022**, *13*, 4875. [CrossRef]
22. Jiang, P.; Ding, W.; Yuan, Y.; Ye, W.; Mu, Y. Interannual variability of vegetation sensitivity to climate in China. *J. Environ. Manag.* **2022**, *301*, 113768. [CrossRef]
23. Yao, Y.; Liu, Y.; Wang, Y.; Fu, B. Greater increases in China's dryland ecosystem vulnerability in drier conditions than in wetter conditions. *J. Environ. Manag.* **2021**, *291*, 112689. [CrossRef] [PubMed]
24. Ran, Y.; Li, X.; Cheng, G. Climate warming over the past half century has led to thermal degradation of permafrost on the Qinghai–Tibet Plateau. *Cryosphere* **2018**, *12*, 595–608. [CrossRef]
25. Zhang, Y.; Li, B.; Zheng, D. A discussion on the boundary and area of the Tibetan Plateau in China. *Geogr. Res.* **2002**, *21*, 1–8. [CrossRef]
26. Ehlers, T.A.; Chen, D.; Appel, E.; Bolch, T.; Chen, F.; Diekmann, B.; Dippold, M.A.; Giese, M.; Guggenberger, G.; Lai, H.; et al. Past, present, and future geo-biosphere interactions on the Tibetan Plateau and implications for permafrost. *Earth-Sci. Rev.* **2022**, *234*, 104197. [CrossRef]
27. Tian, F.; Nan, Y.; Ni, G.; Yang, L.; Tang, Q.; Grey, D. Is the Tibetan Plateau really a water tower? *Hydrol. Process* **2024**, *38*, e15103. [CrossRef]
28. Chen, F.; Wang, Y.; Ding, L.; Yao, T. The expedition and scientific investigation activities on the Tibetan Plateau before 1949. *Acta Geogr. Sin.* **2022**, *77*, 1565–1585. [CrossRef]
29. Yao, T.; Chen, F.; Cui, P.; Ma, Y.; Xu, B.; Zhu, L.; Zhang, F.; Wang, W.; Ai, L.; Yang, X. From Tibetan Pateau to Third Poe and Pan-Third Pole. *Bull. Chin. Acad. Sci.* **2017**, *32*, I0006–I000924.
30. Wang, Y.; Liu, Y.; Chen, P.; Song, J.; Fu, B. Interannual precipitation variability dominates the growth of alpine grassland above-ground biomass at high elevations on the Tibetan Plateau. *Sci. Total Environ.* **2024**, *931*, 172745. [CrossRef]
31. Liu, Y.; Lu, C. Quantifying Grass Coverage Trends to Identify the Hot Plots of Grassland Degradation in the Tibetan Plateau during 2000–2019. *Int. J. Environ. Res. Public Health* **2021**, *18*, 416. [CrossRef] [PubMed]
32. Jiang, Y.; Yang, K.; Qi, Y.; Zhou, X.; He, J.; Lu, H.; Li, X.; Chen, Y.; Li, X.; Zhou, B.; et al. TPHiPr: A long-term (1979–2020) high-accuracy precipitation dataset (1/30°, daily) for the Third Pole region based on high-resolution atmospheric modeling and dense observations. *Earth Syst. Sci. Data* **2023**, *15*, 621–638. [CrossRef]
33. Jiang, Y.; Tang, W.; Yang, K.; He, J.; Shao, C.; Zhou, X.; Lu, H.; Chen, Y.; Li, X.; Shi, J. Development of a high-resolution near-surface meteorological forcing dataset for the Third Pole region. *Sci. China Earth Sci.* **2025**, *68*, 1274–1290. [CrossRef]
34. Kirkland, E.J. *Bilinear Interpolation*; Springer: Boston, MA, USA, 2010; pp. 261–263.
35. Abatzoglou, J.T.; Dobrowski, S.Z.; Parks, S.A.; Hegewisch, K.C. TerraClimate, a high-resolution global dataset of monthly climate and climatic water balance from 1958–2015. *Sci. Data* **2018**, *5*, 170191. [CrossRef]
36. Ding, Y.; Peng, S. Spatiotemporal change and attribution of potential evapotranspiration over China from 1901 to 2100. *Theor. Appl. Clim.* **2021**, *145*, 79–94. [CrossRef]
37. Liu, F.; Wu, H.; Zhao, Y.; Li, D.; Yang, J.; Song, X.; Shi, Z.; Zhu, A.; Zhang, G. Mapping high resolution National Soil In-formation Grids of China. *Sci. Bull.* **2022**, *67*, 328–340. [CrossRef]
38. Li, L. Assessing Anthropogenic and Climatic Impacts on Vegetation Greenness Change on the Tibetan Plateau. Ph.D. Thesis, University of Chinese Academy of Sciences, Beijing, China, 2019.
39. SEN, P.K. Estimates of the Regression Coefficient Based on Kendall's Tau. *J. Am. Stat. Assoc.* **1968**, *63*, 1379–1389. [CrossRef]
40. Mann, H.B. Nonparametric Tests Against Trend. *Econometrica* **1945**, *13*, 245–259. [CrossRef]
41. Breiman, L. Random Forests. *Mach. Learn.* **2001**, *45*, 5–32. [CrossRef]
42. Chen, T.; Guestrin, C. XGBoost: A Scalable Tree Boosting System. In *Proceedings of the 22nd ACM SIGKDD International Conference on Knowledge Discovery and Data Mining, New York, NY, USA, 1 January 2016*; ACM: New York, NY, USA, 2016; pp. 785–794.
43. Vicca, S.; Bahn, M.; Estiarte, M.; van Loon, E.E.; Vargas, R.; Alberti, G.; Ambus, P.; Arain, M.A.; Beier, C.; Bentley, L.P.; et al. Can current moisture responses predict soil CO_2 efflux under altered precipitation regimes? A synthesis of manipulation experiments. *Biogeosciences* **2014**, *11*, 2991–3013. [CrossRef]
44. Grime, J.P. Evidence for the Existence of Three Primary Strategies in Plants and Its Relevance to Ecological and Evolutionary Theory. *Am. Nat.* **1977**, *111*, 1169–1194. [CrossRef]

45. Wu, K.; Chen, J.; Yang, H.; Yang, Y.; Hu, Z. Spatiotemporal Variations in the Sensitivity of Vegetation Growth to Typical Climate Factors on the Qinghai–Tibet Plateau. *Remote Sens.* **2023**, *15*, 2355. [CrossRef]
46. Yao, T.; Thompson, L.G.; Mosbrugger, V.; Zhang, F.; Ma, Y.; Luo, T.; Xu, B.; Yang, X.; Joswiak, D.R.; Wang, W.; et al. Third Pole Environment (TPE). *Environ. Dev.* **2012**, *3*, 52–64. [CrossRef]
47. Kuang, X.; Jiao, J.J. Review on climate change on the Tibetan Plateau during the last half century. *J. Geophys. Res.-Atmos.* **2016**, *121*, 3979–4007. [CrossRef]
48. Mekonnen, Z.A.; Riley, W.J.; Grant, R.F.; Romanovsky, V.E. Changes in precipitation and air temperature contribute comparably to permafrost degradation in a warmer climate. *Environ. Res. Lett.* **2021**, *16*, 24008. [CrossRef]
49. Heikkinen, J.; Keskinen, R.; Kostensalo, J.; Nuutinen, V. Climate change induces carbon loss of arable mineral soils in boreal conditions. *Glob. Change Biol.* **2022**, *28*, 3960–3973. [CrossRef]
50. Piao, S.; Nan, H.; Huntingford, C.; Ciais, P.; Friedlingstein, P.; Sitch, S.; Peng, S.; Ahlström, A.; Canadell, J.G.; Cong, N.; et al. Evidence for a weakening relationship between interannual temperature variability and northern vegetation activity. *Nat. Commun.* **2014**, *5*, 5018. [CrossRef] [PubMed]
51. Wu, K.; Hu, Z.; Wang, X.; Chen, J.; Yang, H.; Yuan, W. Widespread increase in sensitivity of vegetation growth to climate variability on the Tibetan Plateau. *Agric. For. Meteorol.* **2024**, *358*, 110260. [CrossRef]
52. Green, J.K.; Seneviratne, S.I.; Berg, A.M.; Findell, K.L.; Hagemann, S.; Lawrence, D.M.; Gentine, P. Large influence of soil moisture on long-term terrestrial carbon uptake. *Nature* **2019**, *565*, 476–479. [CrossRef]
53. Group, M.R.I.E. Elevation-dependent warming in mountain regions of the world. *Nat. Clim. Change* **2015**, *5*, 424–430. [CrossRef]
54. You, Q.; Chen, D.; Wu, F.; Pepin, N.; Cai, Z.; Ahrens, B.; Jiang, Z.; Wu, Z.; Kang, S.; AghaKouchak, A. Elevation dependent warming over the Tibetan Plateau: Patterns, mechanisms and perspectives. *Earth-Sci. Rev.* **2020**, *210*, 103349. [CrossRef]
55. Liu, L.; Liu, L.; Liang, L.; Donnelly, A.; Park, I.; Schwartz, M.D. Effects of elevation on spring phenological sensitivity to temperature in Tibetan Plateau grasslands. *Chin. Sci. Bull.* **2014**, *59*, 4856–4863. [CrossRef]
56. Huang, M.; Piao, S.; Ciais, P.; Peñuelas, J.; Wang, X.; Keenan, T.F.; Peng, S.; Berry, J.A.; Wang, K.; Mao, J.; et al. Air temperature optima of vegetation productivity across global biomes. *Nat. Ecol. Evol.* **2019**, *3*, 772–779. [CrossRef]
57. Li, W.; Migliavacca, M.; Forkel, M.; Walther, S.; Reichstein, M.; Orth, R. Revisiting Global Vegetation Controls Using Multi-Layer Soil Moisture. *Geophys. Res. Lett.* **2021**, *48*, e2021GL092856. [CrossRef]
58. Peltier, D.M.P.; Ogle, K. Tree growth sensitivity to climate is temporally variable. *Ecol. Lett.* **2020**, *23*, 1561–1572. [CrossRef]
59. Li, M.; Zhang, X.; He, Y.; Niu, B.; Wu, J. Assessment of the vulnerability of alpine grasslands on the Qinghai-Tibetan Plateau. *PeerJ* **2020**, *8*, e8513. [CrossRef] [PubMed]
60. Ran, Q.; Hao, Y.; Xia, A.; Liu, W.; Hu, R.; Cui, X.; Xue, K.; Song, X.; Xu, C.; Ding, B.; et al. Quantitative Assessment of the Impact of Physical and Anthropogenic Factors on Vegetation Spatial-Temporal Variation in Northern Tibet. *Remote Sens.* **2019**, *11*, 1183. [CrossRef]
61. Berisha, N.; Geci, D. The analysis of the influence of grazing intensity on the diversity and abundance of plants and spiders (Arachnida: Araneae). *Eur. J. Environ. Sci.* **2023**, *13*, 31–38. [CrossRef]
62. Dong, J.; Chen, Y.; Yao, B.; Zhang, X.; Zeng, N. A neural network boosting regression model based on XGBoost[Formula presented]. *Appl. Soft Comput.* **2022**, *125*, 109067. [CrossRef]
63. Xiao, L.; Miao, H.; Shi, T.; Hong, Y. LSTM-based deep learning for spatial–temporal software testing. *Distrib. Parallel Databases* **2020**, *38*, 687–712. [CrossRef]

Disclaimer/Publisher's Note: The statements, opinions and data contained in all publications are solely those of the individual author(s) and contributor(s) and not of MDPI and/or the editor(s). MDPI and/or the editor(s) disclaim responsibility for any injury to people or property resulting from any ideas, methods, instructions or products referred to in the content.